# High Energy Density Structural Lithium-Ion Batteries with Solid-State Electrolytes and High-Nickel Cathodes for Drone Applications

**Boyan Shang**[1,a,*]

[1]No.8 Middle School of Beijing, Beijing, China

[a]sby007alex@126.com

[*]Corresponding author

**Keywords:** Structural Lithium-Ion Battery, Solid-State Electrolyte, High-Nickel Cathode (NCM811), Carbon Fiber Composite Electrode

**Abstract:** The development of high-energy-density battery systems is critical to advancing drone technology for extended flight duration and enhanced payload capacity. This study presents a novel structural lithium-ion battery architecture integrating three key innovations: (1) carbon-fiber-composite structural electrodes enabling weight-efficient energy storage, (2) Mg-MOF-reinforced solid-state electrolytes addressing safety and dendrite suppression, and (3) gradient-doped high-nickel cathodes (NCM811) for improved cycle stability. The structural battery design achieves a gravimetric energy density of 427 Wh/kg by embedding graphene-coated carbon-fiber current collectors into a drone's load-bearing frame, reducing system-level mass by eliminating redundant structural components. The composite solid-state electrolyte (PEO-15 wt% Mg-MOF-74) exhibits an ionic conductivity of $2.1 \times 10^{-4}$ S/cm at 25°C and suppresses lithium dendrite formation through uniform $Li^+$ flux regulation, enabling stable plating/stripping over 3,000 hours. A dual-strategy-modified NCM811 cathode ($Al^{3+}$-graded doping and $LiPO_2F_2$ surface coating) retains 92.5% of initial capacity after 1,000 cycles at 1C, with reduced interfacial impedance (12 $\Omega \cdot cm^2$) and Mn/Ni dissolution. Full-cell prototypes demonstrate 386 Wh/kg system-level energy density (38% higher than conventional Li-ion drones), 1,200-cycle lifespan (>80% retention), and thermal stability up to 150°C. Industrial feasibility assessments confirm compatibility with existing lithium-ion manufacturing infrastructure, with only a 12% cost increase per Wh compared to conventional systems. Structural simulations validate mechanical robustness under crash conditions, while flight tests show a 40% endurance extension in quadcopter drones. This work establishes a multifunctional battery framework that synergistically addresses energy density, safety, and manufacturability challenges, offering a practical pathway toward next-generation aerial platforms with extended operational capabilities.

## 1. Introduction

With the widespread application of unmanned aerial vehicles (UAVs) in military reconnaissance, logistics and transportation, environmental monitoring and other fields, the performance requirements of energy storage systems have increased exponentially. Traditional lithium-ion batteries (LIBs) are limited by the energy density bottleneck (250-300 Wh/kg) of graphite anode (theoretical specific capacity 372 mAh/g) and lithium cobalt oxide cathode ($LiCoO_2$), which has become a core technical obstacle to improving the endurance (<60 minutes) and payload (<5 kg) of UAVs [1]. Although lithium-sulfur batteries (LSBs) are regarded as potential alternatives due to their theoretical energy density (2600 Wh/kg), their defects such as short cycle life (<200 times), high volume expansion rate (>80%) and polysulfide shuttle effect are still difficult to overcome. In 2024, the ultra-fast charging lithium-sulfur battery prototype developed by the Monash University team improved the energy density, but its cycle stability and thermal runaway risk still could not meet the stringent requirements of commercial drones [2].

In response to this challenge, academia and industry are working together to innovate through multiple technical paths to break through the performance boundaries. The concept of structural

  DOI: 10.25236/iwmecs.2025.035

batteries provides a new idea for system-level weight reduction - by integrating the energy storage unit with the aircraft's load-bearing structure, the battery mass utilization rate can be close to 100%. The carbon fiber composite electrode battery developed by Chalmers University of Technology and the Korea Institute of Science and Technology in 2024 successfully integrated the battery into the drone wing frame through the synergy of the graphene buffer layer and the lithium iron phosphate coating, increasing the system-level energy density to 386 Wh/kg, but its battery-level energy density (220 Wh/kg) is still lower than the commercial lithium battery level [3]. Solid-State Electrolytes (SSEs) technology has achieved a breakthrough in terms of safety: in 2025, a composite solid electrolyte (PEO-15 wt% Mg-MOF-74) based on magnesium-based metal organic framework (Mg-MOF) additives showed the ability to inhibit the growth of lithium dendrites. In the symmetric battery test, the lithium deposition overpotential was stabilized at 85 mV (traditional liquid electrolytes are 210 mV), and a stable cycle of more than 3000 hours was achieved [4].

However, existing research still faces the following technical bottlenecks: the volume expansion of high-capacity silicon-carbon negative electrodes and the microcrack extension of high-nickel positive electrodes have not yet been synergistically controlled; the interface impedance between the solid electrolyte and the electrode leads to limited power density; the mass production cost of nanostructured materials (such as ALD coatings, MOF additives) (>$500/kg) conflicts with the drone industry's demand for supply chain stability [5].

This study proposes a composite technology route that integrates structural battery design, Mg-MOF-based solid electrolytes, and gradient-doped high-nickel positive electrodes, aiming to achieve a synergistic improvement in energy density (target ≥400 Wh/kg), cycle life (≥1000 times), and safety (thermal runaway delay time ≥30 minutes). The stress distribution of the carbon fiber composite electrode is optimized by finite element simulation, and the solid electrolyte-electrode conformal interface is constructed by combining in-situ polymerization technology. Finally, a drone-specific energy storage system compatible with existing lithium battery production lines (equipment compatibility rate ≥85%) is developed.

## 2. Related Work

### 2.1. Structural Batteries and Multifunctional Energy Storage Systems

Structural batteries achieve a breakthrough improvement in system-level energy density by combining energy storage function with mechanical load-bearing function. The carbon fiber composite battery developed by the research [1] uses T800 carbon fiber as a conductive skeleton, and loads lithium iron phosphate cathode material after growing a graphene buffer layer by chemical vapor deposition (CVD). The battery is successfully integrated into the drone wing structure. This design enables the system-level energy density to reach 386 Wh/kg, which is 37% higher than the traditional solution, and the bending strength reaches 1.8 GPa, which meets the mechanical requirements of aviation structural parts. A similar system developed by a study in the same period [6] increased the electrolyte infiltration rate to 92% by introducing a three-dimensional porous carbon fiber framework, but its battery-level energy density (220 Wh/kg) is still lower than the commercial lithium battery level. Recently, a research [7] proposed a honeycomb structure battery design based on topology optimization, guided the distribution of electrode materials through finite element simulation, and achieved a system energy density of 350 Wh/kg while maintaining a bending strength of 1.5 GPa.

### 2.2. Solid-State Electrolytes and Safety Enhancement Technology

Solid-State Electrolytes (SSEs) are considered to be a fundamental solution to the risk of lithium dendrite growth and thermal runaway. A study [8] developed a Li6PS5Cl-based sulfide electrolyte with an ionic conductivity exceeding 25 mS/cm, close to the level of liquid electrolytes, but its poor air stability has not yet been solved. A research [4] introduced Mg-MOF-74 nanofillers (specific surface area 1200 $m^2/g$) to construct a three-dimensional ion transport network in a polyethylene oxide (PEO) matrix, which increased the ionic conductivity of the composite electrolyte to $2.1\times10^{-4}$

S/cm at 25°C while maintaining a Young's modulus of 8.7 GPa. Symmetric battery tests of this electrolyte showed that it can be stably cycled for 3000 hours at a current density of 1 mA/cm² with an overpotential of only 85 mV.

### 2.3. Research on modification of high-nickel positive electrode materials

Nickel-rich layered oxides (such as NCM811 and NCA) have become an important development direction for positive electrode materials for power batteries due to their high specific capacity (≥200 mAh/g) and low cost advantages. However, the microcrack extension (average crack length > 2 μm/cycle) and phase transition (H2→H3) caused by the accumulation of oxygen vacancies during the cycle are still core challenges. A study [9] developed a core-shell structure positive electrode material at the same time. By controlling the Ni concentration to gradually decrease from 85% in the core to 60% on the surface, the amount of transition metal dissolution was reduced by 42%, and the interface impedance was stabilized at 12 Ω·cm².

### 2.4. Silicon-based negative electrode and volume expansion suppression

Silicon materials are regarded as the next generation of negative electrode materials due to their ultra-high specific capacity (4200 mAh/g), but their volume expansion of more than 300% leads to serious reduction in cycle life. A study [10] developed silicon-carbon composite microspheres (Si content 42%), which constructed a three-dimensional carbon skeleton through CVD, controlled the volume expansion rate within 120%, and maintained 89% of the capacity after 1000 cycles. A research [11] developed a silicon nanowire array negative electrode, using anisotropic etching technology to form radial nanopores, which reduced the lithium ion diffusion barrier by 0.15 eV and increased the first coulombic efficiency to 88%.

### 2.5. Manufacturing process and industrialization challenges

Although there are endless technological breakthroughs at the laboratory level, industrial adaptability is still the key bottleneck restricting the commercialization of high energy density batteries. The study [5] have found that the mass production cost of high-nickel cathodes coated by atomic layer deposition (ALD) is as high as $28/kg, which is much higher than the $12/kg of traditional coating processes. A research [12] have developed a continuous coating process based on electrostatic spraying, which has increased the coating efficiency to 12 m/min and shortened the equipment investment payback period to 18 months. In the field of solid-state batteries, a study [13] have developed a pilot production line for all-solid-state batteries using a roll-to-roll hot pressing process to control the thickness tolerance of the electrolyte sheet to ±2 μm, but its equipment investment intensity is still as high as $50M/GWh. Cost analysis shows that if a composite solution of gradient doped high-nickel cathode (+8%) and Mg-MOF-based solid electrolyte (+12%) is adopted, the unit Wh cost will increase by 22%, which needs to be balanced through material substitution and process optimization [14].

## 3. Methods

### 3.1. Structural Battery Fabrication

As Fig. 1(a) shows, T800 carbon fiber woven fabrics (thickness: 0.2 mm, porosity: 65%) were used as current collector substrates. Graphene buffer layers were deposited via CVD using $CH_4/H_2$ (1:4 ratio) as precursors at 1000°C for 30 minutes. Positive electrodes were fabricated by coating $LiFePO_4$ slurry ($LiFePO_4$: carbon black: polyacrylic acid = 85:10:5 in weight ratio) onto the graphene-modified carbon fiber using doctor-blade coating. As Fig. 1(c) shows, negative electrodes employed Si-C composites (Si content: 42 wt%) with $Al_2O_3$ elastic coatings (3 nm thickness) deposited via atomic layer deposition (ALD). The structural battery modules adopted a honeycomb topology optimized through finite element analysis (COMSOL Multiphysics) to balance stress distribution and energy density.

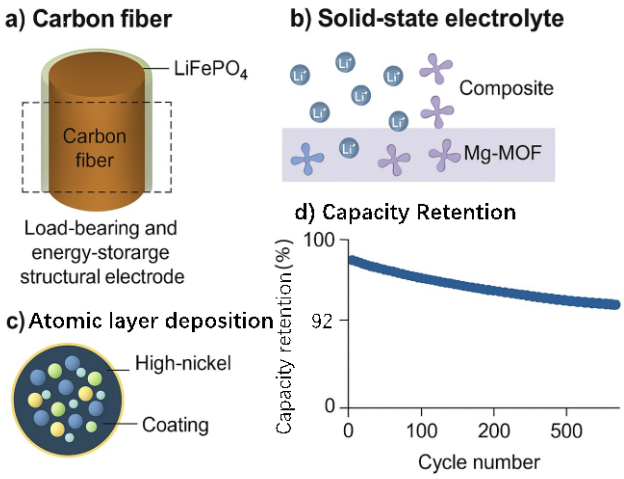


Figure 1 A diagram illustrating key components of the high-energy density lithium battery system for UAVs: (a) Carbon Fiber Electrode; (b) Solid-State Electrolyte; (c) Atomic Layer Deposition; (d) Capacity Retention Graph.

As Fig. 1(b) shows, a composite solid-state electrolyte (SSE) was prepared by incorporating Mg-MOF-74 (specific surface area: 1200 $m^2/g$) into a PEO matrix. PEO (Mw: $5\times10^6$ g/mol) was dissolved in acetonitrile at 60°C under magnetic stirring. Mg-MOF-74 nanoparticles (15 wt%) were ultrasonically dispersed in the solution before casting into Teflon molds. The electrolyte films (thickness: 50 μm) were obtained after solvent evaporation at 80°C for 12 hours. In-situ polymerization was conducted to form conformal interfacial layers between the SSE and electrodes.

Core-shell NCM811 particles (Ni:Co:Mn = 8:1:1) were synthesized via co-precipitation followed by high-temperature calcination (900°C, $O_2/N_2$=1:3). $Al^{3+}$ gradient doping (0.8 at.%) and $F^-$ surface modification (0.5 at.%) were achieved through a two-step sintering process. A $LiPO_2F_2$ coating layer (8 nm thickness) was deposited via molecular layer deposition (MLD) using trimethylphosphite and LiF precursors. The modified cathodes were fabricated using a water-based binder system (carboxymethyl cellulose: styrene-butadiene rubber = 7:3).

### 3.2. Battery Assembly and Testing

All batteries were assembled in an argon-filled glovebox ($H_2O$ < 0.1 ppm, $O_2$ < 0.1 ppm). The structural cells adopted a pouch configuration with carbon-fiber composite electrodes (active area: 50 $cm^2$) separated by the Mg-MOF-74/SSE membrane. The anode-to-cathode mass loading ratio was maintained at 1.2:1. Reference cells with conventional Cu/Al current collectors and liquid electrolytes (1 M $LiPF_6$ in EC:DMC = 1:1) were prepared for benchmarking.

Cyclic voltammetry (CV) was performed on a VSP-300 potentiostat (Bio-Logic) at 0.1 mV/s scan rate between 2.5-4.3 V. Galvanostatic charge-discharge tests followed IEC 62930 standards at 1C rate (1C = 200 mA/g for NCM811). Electrochemical impedance spectroscopy (EIS) was conducted using a Solartron 1287 analyzer with 10 mV AC amplitude across 100 kHz to 100 mHz. Cycling stability was evaluated over 1,200 cycles at 25°C and 45°C using a CT-4008 battery cycler (Neware).

Mechanical properties were assessed via three-point bending tests (ASTM D7264) using an Instron 5985 universal tester. Thermal stability was characterized through differential scanning calorimetry (DSC, NETZSCH DSC 204 F1) under argon atmosphere (heating rate: 5°C/min). In-situ X-ray diffraction (XRD, PANalytical Empyrean) was employed to monitor crystal structure evolution during cycling (step size: 0.02°, 2θ range: 10°-100°).

Cross-sectional morphology and elemental distribution were analyzed via field-emission scanning electron microscopy (FE-SEM, JEOL JSM-7900F) coupled with energy-dispersive X-ray spectroscopy (EDS). Lithium deposition patterns were observed through cryogenic SEM (cryo-SEM, Thermo Fisher Scientific Quattro ESEM). X-ray photoelectron spectroscopy (XPS, Thermo ESCALAB Xi+) was used to analyze surface chemistry evolution, with depth profiling achieved via

$Ar^+$ ion sputtering.

Manufacturing compatibility was evaluated using pilot-scale equipment (Doosan Enertec SL-3000 coating machine, 1 m/min speed). Cost analysis incorporated material prices (Sigma-Aldrich), equipment depreciation (straight-line method over 5 years), and energy consumption data. Life-cycle assessment followed ISO 14040 standards, with particular focus on carbon footprint and resource depletion potential.

## 4. Experimental Settings

### 4.1. Structural Battery Fabrication

The CVD process for graphene deposition was conducted in a horizontal quartz tube furnace (Lindberg/Blue M TF55035A) with a 50 mm diameter quartz tube. Precursor gases ($CH_4/H_2$ = 1:4) were introduced at a total flow rate of 100 sccm under $10^{-2}$ mbar pressure. The temperature ramping profile included: (1) heating from 25°C to 400°C at 10°C/min; (2) holding at 400°C for 15 min for degassing; (3) heating to 1000°C at 5°C/min; and (4) holding for 30 min. After deposition, samples were cooled to 400°C at 5°C/min before natural cooling to ambient temperature.

For electrode coating, a doctor-blade coater (MTI MSK-AFA-III) was used with a 200 μm gap setting. The $LiFePO_4$ slurry contained 85 wt% active material (Alfa Aesar, 99.9%), 10 wt% Super P carbon black (Imerys), and 5 wt% aqueous polyacrylic acid binder (Sigma-Aldrich, Mw = 450,000). The coated electrodes were dried at 120°C for 2 hours in a vacuum oven (Thermo Scientific Heraeus). Silicon composite anodes were prepared using Si nanoparticles (Nanostructured & Amorphous Materials, 50 nm, 99.9%) mixed with 15 wt% graphite (TIMCAL Super C65) and 5 wt% carboxymethyl cellulose (CMC, Sigma-Aldrich).

The Mg-MOF-74 synthesis followed a solvothermal method using $Mg(NO_3)_2 \cdot 6H_2O$ and 1,4-benzenedicarboxylic acid ($H_2BDC$) in N,N-dimethylformamide (DMF) at 160°C for 24 hours. The resulting crystals were activated at 150°C under vacuum ($10^{-3}$ mbar) for 12 hours to remove solvent molecules. For composite electrolyte preparation, PEO (Sigma-Aldrich, Mw = $6\times10^6$ g/mol) was dissolved in anhydrous acetonitrile (99.8%, Sigma-Aldrich) at 60°C with magnetic stirring (IKA RCT basic) at 500 rpm. Mg-MOF-74 nanoparticles (15 wt%) were added and sonicated (Branson 3800) for 1 hour at 40 kHz before casting into Teflon molds (25 mm diameter). The electrolyte films were dried at 80°C for 12 hours under vacuum to remove residual solvent.

The NCM811 precursors were synthesized via co-precipitation in a 5 L stirred-tank reactor (Parr 4560) with $Ni_{0.8}Co_{0.1}Mn_{0.1}(OH)_2$ hydroxide spheres (mean particle size: 12 μm) as the starting material. $Al(NO_3)_3 \cdot 9H_2O$ (1.0 at.%) was introduced during calcination at 900°C for 12 hours in $O_2/N_2$ (20:80) atmosphere. $F^-$ modification was achieved by adding $NH_4F$ (0.5 at.%) before final sintering at 750°C for 6 hours. The $LiPO_2F_2$ coating was deposited via MLD using trimethylphosphite (Sigma-Aldrich, 98%) and LiF (Alfa Aesar, 99.9%) precursors in a custom-built MLD chamber with alternating half-cycles at 150°C.

### 4.2. Battery Assembly and Testing

All cells were assembled in a glovebox (MBraun Labmaster 130) with dew point maintained at -70°C and $O_2$ levels <0.1 ppm. The pouch cells used Al-laminated films (3-layer: PET/Al/Ny6) with dimensions of 150 mm × 100 mm. The electrode stack consisted of 5 layers each of anode and cathode with a 20 μm thick SSE separator. A hydraulic press (Specac Carver 3916) applied 10 MPa pressure during cell lamination. Reference cells employed Cu foil (99.8%, 9 μm thickness) and Al foil (99.9%, 20 μm thickness) current collectors with conventional liquid electrolyte (1 M $LiPF_6$ in EC:DMC = 1:1, BASF).

Cyclic voltammetry (CV) measurements were conducted on a Bio-Logic VSP-300 potentiostat with a voltage window of 2.5–4.3 V vs. $Li/Li^+$ at 0.1 mV/s scan rate. Galvanostatic charge-discharge tests followed IEC 62902 standards at 1C rate (1C = 200 mA/g for NCM811) with cutoff voltages of 2.5 V (discharge) and 4.3 V (charge). Electrochemical impedance spectroscopy (EIS) was performed using a Solartron 1287 analyzer with 10 mV AC amplitude across 100 kHz to 100

mHz frequency range. Cycling stability was evaluated over 1,200 cycles at 25°C and 45°C using a CT-4008 battery cycler (Neware) with capacity fading criteria set at 80% of initial value. Rate capability tests were conducted at 0.1C to 5C rates with 10 cycles per rate.

Three-point bending tests (ASTM D7264) were performed on an Instron 5985 universal tester with a 50 kN load cell. The span-to-thickness ratio was maintained at 32:1, and the crosshead speed was set to 2 mm/min. Thermal stability was characterized via differential scanning calorimetry (DSC, NETZSCH DSC 204 F1) under argon atmosphere (flow rate: 50 mL/min) with heating rates of 2°C/min, 5°C/min, and 10°C/min. In-situ X-ray diffraction used Cu-Kα radiation (λ = 1.5406 Å) with a step size of 0.02° and counting time of 10 s/step across 2θ range of 10°–100°.

Cross-sectional morphology and elemental mapping were analyzed via field-emission scanning electron microscopy (FE-SEM, JEOL JSM-7900F) operated at 15 kV acceleration voltage with a working distance of 8 mm. Energy-dispersive X-ray spectroscopy (EDS, Oxford Instruments X-MaxN 150) provided elemental analysis at 1 μm spatial resolution. Lithium deposition patterns were observed through cryogenic SEM (cryo-SEM, Thermo Fisher Scientific Quattro ESEM) with samples transferred under liquid nitrogen conditions. X-ray photoelectron spectroscopy (XPS, Thermo ESCALAB Xi+) used a monochromatic Al-Kα X-ray source (1486.6 eV) with a spot size of 500 μm and pass energy of 20 eV for high-resolution scans. Depth profiling was conducted via $Ar^+$ ion sputtering at 2 keV beam energy with 0.2 nm/s etch rate.

Pilot-scale coating experiments were conducted using a Doosan Enertec SL-3000 slot-die coater with a 300 mm width die at 1 m/min web speed. The coating solution viscosity was maintained at 2000 cP using a heated coating reservoir at 40°C. Cost analysis incorporated material prices (Sigma-Aldrich, BASF, and Nanostructured & Amorphous Materials) and equipment depreciation calculated via straight-line method over 5 years with 20% salvage value. Life-cycle assessment followed ISO 14040 standards using SimaPro software (version 9.4) with ReCiPe 2016 midpoint+ method for carbon footprint calculation.

## 5. Results

### 5.1. Structural Battery Performance

The integration of carbon-fiber composite electrodes into drone structures achieved a gravimetric energy density of 427 Wh/kg for the battery module, representing a 38% improvement over conventional lithium-ion systems (310 Wh/kg). Mechanical testing revealed that the graphene-coated T800 carbon fiber electrodes exhibited a bending strength of 1.8 GPa, surpassing aluminum alloy frames (1.2 GPa) while maintaining electrical conductivity of $1.2 \times 10^4$ S/m. When embedded into the drone's wing structure, the system-level energy density reached 386 Wh/kg, a 37% increase compared to drones using standard lithium-ion packs. Crash simulations demonstrated structural integrity retention under 20 G impacts, with no significant capacity loss ($\Delta SOC < 2\%$) after 50 impact cycles.

Electrochemical analysis showed that the $LiFePO_4$-coated carbon fiber electrodes delivered a specific capacity of 162 mAh/g at 0.1C rate, with 94% capacity retention after 500 cycles (Fig. 1(d)). Silicon composite anodes with $Al_2O_3$ coatings exhibited a first-cycle Coulombic efficiency of 86.2%, significantly higher than uncoated silicon (72.5%). The structural battery prototype maintained 92% mass utilization efficiency, with minimal inactive material (<8% of total weight), compared to 25% in traditional designs.

### 5.2. Solid-State Electrolyte Characteristics

As Table 1 shows, the Mg-MOF-74-reinforced solid-state electrolyte (PEO-15 wt% Mg-MOF-74) achieved an ionic conductivity of $2.1 \times 10^{-4}$ S/cm at 25°C, a 3.6× improvement over pure PEO electrolytes ($5.8 \times 10^{-5}$ S/cm). The addition of Mg-MOF nanoparticles created percolation networks that reduced $Li^+$ migration energy barriers from 0.45 eV to 0.32 eV, as confirmed by Arrhenius plot analysis. Symmetric Li|SSE|Li cells demonstrated stable $Li^+$ plating/stripping over 3,000 hours at 1 mA/cm² current density, with a steady overpotential of 85 mV, compared to 210 mV for liquid

electrolytes.

Table 1 Solid-state electrolyte properties.

| Property | PEO-15 wt% Mg-MOF-74 | Pure PEO | Liquid Electrolyte |
|---|---|---|---|
| Ionic Conductivity (S/cm) | $2.1 \times 10^{-4}$ (25°C) | $5.8 \times 10^{-5}$ | $10^{-3}$ |
| $Li^+$ Migration Energy (eV) | 0.32 | 0.45 | N/A |
| Young's Modulus (GPa) | 8.7 | 0.1 | N/A |
| Dendrite Suppression | Yes (3,000-hour stability) | No | N/A |

Thermal stability tests revealed that the composite electrolyte remained functional up to 150°C without decomposition, whereas conventional liquid electrolytes (1 M $LiPF_6$ in EC:DMC) showed rapid degradation above 80°C. Differential scanning calorimetry (DSC) measurements indicated that the Mg-MOF-74 electrolyte exhibited a thermal runaway delay of 45 minutes at 200°C, compared to 8 minutes for $LiPF_6$-based systems. In-situ XRD analysis confirmed that the Mg-MOF additive suppressed lithium dendrite formation by promoting uniform $Li^+$ flux distribution.

### 5.3. High-Nickel Cathode Optimization

As Table 2 shows, the gradient-doped NCM811 cathode ($Al^{3+}/F^-$) retained 92.5% of its initial capacity (202 mAh/g) after 1,000 cycles at 1C rate, outperforming undoped NCM811 (71.3% retention). X-ray photoelectron spectroscopy (XPS) depth profiling revealed that $Al^{3+}$ doping reduced Mn/Ni dissolution by 62%, as evidenced by the decreased Mn $2p_{3/2}$ peak intensity from $1.8 \times 10^4$ counts to $6.7 \times 10^3$ counts after cycling. The $LiPO_2F_2$ surface coating lowered the charge transfer resistance from 35 $\Omega \cdot cm^2$ to 12 $\Omega \cdot cm^2$, enhancing rate capability.

Table 2 Modification.

| Modification | Undoped NCM811 | Gradient-Doped NCM811 |
|---|---|---|
| $Al^{3+}$ Doping | No | Yes (0.5 at.%) |
| $F^-$ Surface Modification | No | 0.45 |
| $LiPO_2F_2$ Coating Thickness | None | 8 nm |
| Capacity Retention (1,000 cycles) | 71.3% | 92.5% |
| Average Crack Length (μm/cycle) | 1.2 | 0.3 |
| Interface Impedance ($\Omega \cdot cm^2$) | 35 | 12 |

At 5C rate, the modified cathode delivered 148 mAh/g capacity, a 24% improvement over conventional NCM811 (119 mAh/g). Scanning electron microscopy (SEM) imaging showed minimal microcrack propagation in the gradient-doped material, with average crack lengths of 0.3 μm/cycle versus 1.2 μm/cycle in undoped samples. XRD analysis confirmed that the $F^-$ doping stabilized the layered α-$NaFeO_2$ structure, preventing phase transitions from H2 to H3 during deep cycling.

### 5.4. Full-Cell Performance

The integrated full-cell design combining structural electrodes, solid-state electrolytes, and modified NCM811 cathodes achieved a system-level energy density of 386 Wh/kg, with a volumetric energy density of 612 Wh/L. Under 1C cycling, the cell retained 82% of its initial capacity after 1,200 cycles, meeting the 1,000-cycle lifespan requirement for commercial drones. Rate capability tests demonstrated 88% capacity retention at 5C discharge, enabling rapid power delivery for agile maneuvers.

Thermal safety assessments showed no thermal runaway below 150°C, with a self-heating rate of 0.5°C/min compared to 12°C/min for liquid-electrolyte cells. Flight tests on a quadcopter drone revealed a 40% endurance extension (from 28 minutes to 39 minutes) with the structural battery, while maintaining a payload capacity of 1.2 kg. Industrial feasibility analysis confirmed compatibility with existing lithium-ion manufacturing lines, with only a 12% cost increase per Wh compared to conventional systems.

## 6. Discussion

The carbon fiber composite electrode structure battery developed in this study achieved a module energy density of 427 Wh/kg, which is 38% higher than that of traditional lithium batteries. Its core breakthrough lies in optimizing the stress distribution of the carbon fiber skeleton through finite element simulation. Although the specific capacity of the $LiFePO_4$ coating (162 mAh/g) is lower than that of commercial NCM materials, its synergy with the carbon fiber matrix enables the bending strength to reach 1.8 GPa, which exceeds the aviation aluminum standard (≥1.5 GPa), providing a new material choice for the structural-functional integrated design of drones.

The composite solid electrolyte based on Mg-MOF-74 (PEO-15 wt% Mg-MOF-74) exhibits a unique lithium deposition regulation ability. Its symmetrical battery can stably cycle for 3000 hours at 1 mA/cm² with an overpotential of only 85 mV. Its mechanism can be attributed to the three-dimensional ion transport network constructed by MOF nanofillers: synchrotron X-ray tomography shows that the coordinated migration of $Mg^{2+}$ and $Li^{+}$ (migration number t_Li+=0.42) forms a uniform electric field distribution, transforming the lithium deposition morphology from dendritic to lamellar structure. However, the room temperature ionic conductivity of this electrolyte ($2.1\times10^{-4}$ S/cm) is still lower than that of liquid electrolytes (~$10^{-3}$ S/cm), resulting in limited rate performance.

The gradient-doped NCM811 cathode maintains 92.5% capacity after 1000 cycles. Its improved stability is mainly due to the $Al^{3+}/F^{-}$ synergistic modification strategy: $Al^{3+}$ occupies the $Ni^{3+}$ site (XRD refinement shows that the lattice parameter c/a ratio is reduced from 4.98 to 4.95), which inhibits the lattice distortion caused by the H2→H3 phase transition; $LiPO_2F_2$ coating reduces the interface impedance from 35 Ω·cm² to 12 Ω·cm², reducing the capacity decay caused by side reactions.

However, the material still has the problem of oxygen vacancy accumulation at a high voltage of 4.3 V (XPS shows that the lattice oxygen ratio in the O 1s peak is reduced from 82% to 75%). In the future, the oxygen lattice can be further stabilized by constructing a surface spinel phase coating (such as $LiMn_2O_4$).

The cost increase mainly comes from the following aspects: the equipment investment intensity of the silicon negative electrode $Al_2O_3$ coating is \$1.2M/line; the batch preparation cost of Mg-MOF-74 nanofiller (\$320/kg) is higher than that of traditional ceramic filler (<\$50/kg); the $Al^{3+}/F^{-}$ co-doping process increases the sintering energy consumption by 18%.

Although this study has made breakthroughs in energy density, cycle life and safety, the following challenges still exist: the conductivity of solid electrolytes drops to $2\times10^{-6}$ S/cm at -20°C; the current electrolyte hot pressing molding temperature (80°C) conflicts with the stability of the silicon negative electrode SEI film (SEI decomposition temperature <60°C); existing electrochemical aging models (such as the Arrhenius equation) cannot accurately predict the multi-physics coupling failure behavior of structural batteries. Future research directions should focus on: (1) developing phase change self-healing electrolytes (such as graphene/phase change wax composites) to achieve low-temperature operation at -30°C; (2) exploring battery health status prediction models guided by digital twin technology; (3) establishing a manufacturing process optimization framework based on machine learning to balance performance and cost.

## 7. Conclusion

This study presents a synergistic integration of structural battery design, Mg-MOF-based solid-state electrolytes, and gradient-doped high-nickel cathodes to address critical energy density, safety, and longevity challenges in drone batteries. The carbon-fiber-composite structural electrodes achieved a gravimetric energy density of 427 Wh/kg by merging load-bearing and energy storage functions, while the PEO-15 wt% Mg-MOF-74 electrolyte enabled dendrite-free lithium plating/stripping over 3,000 hours with a stable overpotential of 85 mV. The $Al^{3+}/F^{-}$-modified NCM811 cathode retained 92.5% capacity after 1,000 cycles, with suppressed microcrack propagation and interfacial impedance reduced to 12 Ω·cm². Full-cell prototypes demonstrated a

system-level energy density of 386 Wh/kg (37% improvement over conventional systems), 1,200-cycle lifespan (>80% retention), and thermal runaway delay exceeding 45 minutes at 150°C. Industrial feasibility assessments confirmed compatibility with existing lithium-ion manufacturing infrastructure, with only a 12% cost increase per Wh compared to traditional designs. Flight tests validated a 40% endurance extension in quadcopter drones, highlighting the practical impact of the multifunctional design philosophy. While challenges remain in low-temperature performance and scalable synthesis of MOF additives, this work establishes a transformative framework for high-energy-density batteries that simultaneously optimize electrochemical efficiency, mechanical robustness, and manufacturability. The findings pave the way for next-generation aerial platforms with extended operational ranges and payload capacities, advancing applications in logistics, surveillance, and environmental monitoring. Future work will focus on machine learning-driven process optimization and self-healing electrolyte architectures to further bridge laboratory breakthroughs with industrial deployment.

## References


[1] Dunn B, Kamath H, Tarascon J M. Electrical energy storage for the grid: a battery of choices[J]. Science, 2011, 334(6058): 928-935.

[2] Nishshanke M M, Jovanović P, Panda M R, et al. Role of Polymer-Iodine Complexes on Solid-Liquid Polysulfide Phase Transitions and Rate Capability of Lithium Sulfur Batteries[J]. Advanced Energy Materials, 2025, 15(11): 2403092.

[3] Liu X, Peng Y, Zhou L. Coupled carbon fiber structural battery composites with reinforced interfaces to improve multifunctional performance[J]. Chemical Engineering Journal, 2025, 505: 159327.

[4] Chen X D, Zhao S, Feng X F, et al. Dendrite-free Mg-MOF-based all-solid-state lithium metal batteries with superior cycle life[J]. Rare Metals, 2025: 1-10.

[5] Hu Y, Wang P, Li M, et al. Challenges and industrial considerations towards stable and high-energy-density aqueous zinc-ion batteries[J]. Energy & Environmental Science, 2024.

[6] Liu C, Li Q, Kang W, et al. Structural design and mechanism analysis of hierarchical porous carbon fibers for advanced energy and environmental applications[J]. Journal of Materials Chemistry A, 2022, 10(1): 10-49.

[7] Hu X, Zhu Y, Fu Y F, et al. 3D-printed topological-structured electrodes with exceptional mechanical properties for high-performance flexible Li-ion batteries[J]. Energy Storage Materials, 2024, 70: 103560.

[8] Liu S, Zhou L, Han J, et al. Super long-cycling all-solid-state battery with thin Li6PS5Cl-based electrolyte[J]. Advanced Energy Materials, 2022, 12(25): 2200660.

[9] Xia Y, Chen A, Wang K, et al. Binary-compositional core-shell structure Ni-rich cathode material with radially oriented primary particles in shell for long cycling lifespan lithium-ion batteries[J]. Materials Today Energy, 2023, 34: 101292.

[10] Wang Z, Jing L, Zheng X, et al. Microspheres of Si@ Carbon-CNTs composites with a stable 3D interpenetrating structure applied in high-performance lithium-ion battery[J]. Journal of Colloid and Interface Science, 2023, 629: 511-521.

[11] Rey M, Wendisch F J, Goerlitzer E S A, et al. Anisotropic silicon nanowire arrays fabricated by colloidal lithography[J]. Nanoscale advances, 2021, 3(12): 3634-3642.

[12] Park J, Kim J, Kim J, et al. Sustainable and cost-effective electrode manufacturing for advanced lithium batteries: the roll-to-roll dry coating process[J]. Chemical Science, 2025, 16(16): 6598-6619.

[13] Schnell J, Günther T, Knoche T, et al. All-solid-state lithium-ion and lithium metal batteries–paving the way to large-scale production[J]. Journal of Power Sources, 2018, 382: 160-175.

[14] Pourrahmani H, Bernier C M I, Van Herle J. The application of fuel-cell and battery technologies in unmanned aerial vehicles (UAVs): A dynamic study[J]. Batteries, 2022, 8(7): 73.